
Proceedings Paper:
Monoranu, M., Ashworth, S. orcid.org/0000-0003-1192-6127, M'Saoubi, R. et al. (5 more authors) (2019) A comparative study of the effects of milling and abrasive water jet cutting on flexural performance of CFRP. In: Kerrigan, K., Mativenga, P. and El-Dessouky, H., (eds.) Procedia CIRP. 2nd CIRP Conference on Composite Material Parts Manufacturing, 10-11 Oct 2019, Advanced Manufacturing Research Centre, UK. Elsevier , pp. 277-283.

https://doi.org/10.1016/j.procir.2019.09.036

Available online at www.sciencedirect.com

ScienceDirect

Procedia CIRP 85 (2019) 277–283

www.elsevier.com/locate/procedia

2nd CIRP Conference on Composite Material Parts Manufacturing (CIRP-CCMPM 2019)

A comparative study of the effects of milling and abrasive water jet cutting on flexural performance of CFRP

Marius Monoranu[a,c,*], Sam Ashworth[a,c], Rachid M'Saoubi[d], J. Patrick Fairclough[c], Kevin Kerrigan[b], Richard J. Scaife[b], Sam Barnes[c] , Hassan Ghadbeigi[c]

[a]*Industrial Doctoral Centre in Machining Science, Advanced Manufacturing Research Centre, University of Sheffield, Rotherham, S60 5TZ, United Kingdom*
[b]*Advanced Manufacturing Research Centre, The University of Sheffield, Rotherham S60 5TZ, United Kingdom*
[c] *Department of Mechanical Engineering, The University of Sheffield, Sheffield, S1 3JD, United Kingdom*
[d] *Materials & Technology Development, Seco Tools AB, SE73782 Fagersta, Sweden*

* Corresponding author. Tel.: +44-745-501-4034; *E-mail address:* m.monoranu@sheffield.ac.uk

Abstract

Machining of carbon fibre reinforced polymers is part of the production process that introduces several challenges due to inherent characteristics of CFRPs such as non-homogeneity of their mechanical properties. A comparative analysis of conventional milling and abrasive water jet (AWJ) cutting is performed to quantify the effects of machining induced damage on flexural strength of woven CFRP laminates. The machined surfaces quality is characterized using optical and scanning electron microscopy methods prior to flexural mechanical testing. High-speed Digital Image Correlation technique is also used to measure deformation evolutions and determine fracture mechanisms in relation to the applied machining operation and produced machined surfaces. The effect of machining induced damage on strength of milled samples was less than expected with the AWJ processed samples having the least mechanical properties. The surface morphology analysis revealed that the entry and exit point of the water jet introduced severe surface and subsurface damage across the full thickness. The failure initiation sites were determined by strain distribution maps indicating that machining induced damage promotes failure of the tested CFRPs away from maximum compressive stress observed under the loading points.

Keywords: composite, machining, damage, milling, waterjet machining

1. Introduction

CFRPs are increasingly used for structural components of aircrafts and high performance automotive applications due to their high strength to weight ratio. CFRP parts are usually trimmed after production or holes are made to them for the ease of assembly. The machining of CFRPs introduces several challenges due to their anisotropic and inhomogeneous state as well as the presence of very abrasive fibres. Application of conventional and non-conventional machining processes including milling [1-3] and Abrasive Water Jet Machining (AWJM) [4-8] on CFRPs have already been studied by many researchers. These mostly cover the mechanics of material removal due to the interaction of solid cutting tool and material removal process in AWJM. Additionally, the effects of selected cutting parameters on developed machining induced damage such as delamination; fibre rupture and pull-out; matrix burning and smearing have also been studied [9]. A rapid tool wear is reported in milling of CFRPs due to the abrasive nature of carbon fibres leading to increased cutting forces and deteriorated surface quality [10]. It is reported that surface roughness decreases with an increase in cutting speed and increases with an increase in feed rate during composite machining [11, 12]. Surface roughness has also been used as an indicator of machining induced damage in CFRPs that is adversely affecting the structural integrity and functional performance of the produced parts [9, 12-14]. Ghidossi et al. [12] studied the influence of milling and AWJM on mechanical

2212-8271
10.1016/j.procir.2019.09.036

properties of composite coupons. No conclusive results were reported mainly due to the difficulties associated with correlation of microscopic observations with general behaviour of the material tested. On the other hand, surface roughness affected the fatigue life of machined composite panels after AWJM and burr tool machining [13]. The effects of three machining operations (Abrasive Water Jet (AWJ), circular diamond saw and shaper planer mounted with polycrystalline diamond tool inserts) on the mechanical flexural properties of graphite/epoxy laminate samples were studied by Arola and Ramulu [15]. According to the reported findings, no representative difference was found in the bulk strength of the laminates under bending loads, however a peak load difference was observed.

To overcome the issues related to the tool wear and subsequent surface quality deterioration, AWJM is increasingly implemented in cutting CFRPs [4-8, 16-19]. Ramulu and Arola Arola [4, 8, 16] studied the AWJ process of CFRP in a series of experiments. A combination of shearing, micromachining and erosion mechanisms [16] lead to the development of three main damage zones at the entry of the jet, a cutting wear zone and a deformation zone near the exit of the jet at the machined kef wall. Doreswamy et al. [17] reported that the kerf width increases with an increase in operating pressure and standoff distance, but decreased with an increase in feed rate when machining GFRP. Similar results were found by Hofy et al. [5] when machining two types of CFRP lay-ups. Another study [19] concluded that the grit size is the most significant process factor which affected the surface finish and kerf taper size. The general conclusion is that in order to obtain a good surface quality, high operating pressure, low feed rate and small standoff distances should be used in AWJM of CFRPs.

There are several reports available in which the field deformation distributions within composite materials have been measured, however these are mostly limited to the fracture mechanics investigations [20-22] and the fibre orientation effects on flexural behaviour of E-glass/polyester pultruded composites [23]. However, limited knowledge and understanding is available on the effect of machining operations on deformations field of CFRPs.

This paper investigates the effects of machining induced damage on flexural behaviour, crack propagation and resultant failure modes of CFRP laminates subjected to 4-point bending. Flexural tests are coupled with high-speed Digital Image Correlation (DIC) measurements in order to quantify the effects of machining induced damage on the deformation evolution and fracture mechanics of samples generated by each machining operation combined with high speed DIC analysis.

2. Project methodology

2.1. CFRP panel manufacture and characterisation

Two, 300 x 300 x 3 mm CFRP panels were manufactured using a Hypaject Mk I RTM system. A diglycidyl-ether-of-bisphenol-F (DGEBF) PY 306 epoxy (Atalanta, UK) and triethylenetetramine (TETA) hardener (Sigma Aldrich, UK) were mixed at a stoichiometric ratio of 100 parts epoxy to 15 parts hardener by mass. 14 plies of M46JB 6K 50B, 223 GSM, 2 x 2 twill woven fibres (Sigmatex, UK) were stacked in a (0,90) orthotropic lay-up. Manufacturing process was followed according to Ashworth et al. [24].

Two random sections from each panel were cut to determine the fibre-volume fraction prior to machining to ensure a similar content across all panels was achieved. The samples were prepared according to Ashworth et al. [25]. The ratio of matrix, void and fibres was calculated through contract analysis of five different pictures using Pax-it! 2 software (USA). The measured values were averaged and reported for further investigations.

2.2. Machining of the test samples

Three sets of samples were produced, one with milled edges, one cut by AWJ and a set with milled edges were the machining induced damage was removed by polishing and grinding. The latter served as the reference set to compare flexural strength of the produced samples. A XYZ 1060HS VMC 3-axis milling machine together with a 6mm SecoTools JC 871060 uncoated burr tool were used to trim the produced CFRP panels where the panels were attached to a specially designed aluminum tooling block. A Karcher 001 NT 35/1 Tact Te H extraction system is used to remove hazardous dust with the extraction nozzle placed locally near the cutting area. The selected parameters chosen according to the tool manufacturer recommendations to obtain a high quality surface finish are shown in Table 1.

Table 1. Milling tool parameters

Type	Cutting diameter (6 mm)	Cutting speed (m/min)	Feed per teeth (mm/tooth)	Feed rate (mm/min)	RPM
JC 871060	6	120	0.012	764	6366

A Protomax (Omax, USA) AWJ machine was also used to cut the required test coupons. CFRP panels were submerged 1 mm under water during cutting. The water pressure and feed rate of the nozzle was set based on type and thickness of material and a level of desired surface quality. Although, fine tuning of the parameters were not available on this machine, the aim was to obtain a good surface finish, therefore the input parameters were set to obtain maximum performance from the AWJ cutter. Process parameters are listed in Table 2.

Table 2. AWJ machining parameters

Pressure (MPa)	Nozzle orifice (mm)	Focusing tube (mm)	Stand of distance (mm)	Feed rate (mm/min)	Abrasive mesh size (AquaJet, UK)
204	0.2	0.762	1.3	310	80

Machined surfaces of the third set of samples were polished to remove any defects induced by the machining process. Polishing was done using CarbiMet Plain P800 (Buehler, UK) to obtain a uniform surface finish after removing of 0.2 mm by

which the material was inspected and it was not affected by the edge trimming process.

2.3. Post-machining assessment

Areal surface scanning was conducted using an Alicona Infinite Focus SL optical focus variation system using 10x magnification. Exposure was set to 7.25 ms and contrast set to 0.7 with vertical resolution and lateral resolution set to 400nm and 1µm. An area with a length of 8 mm on the machined side of the samples was scanned covering 8 x 3 mm^2 with 3 mm to be the thickness of the sample. A cut off length λ_c of 0.8 mm was applied to the image before spatial and autocorrelation textural parameters were collected from Alicona IF-Measurement Suite. Profile data was collected and measured according to ISO 4288 [26] and ISO 3274 [27] specifications. Five measurements were taken in the transverse cutting direction across the full thickness of the sample.

A FEI Inspect F FEG-SEM was used to assess the machined surface morphology at high magnification. Samples were gold-coated prior to the SEM microscopy for the better conductivity.

2.4. Mechanical testing

Four point bend flexural tests were performed in accordance to ASTM D6272 [28]. A load span of one half of the support span was selected to ensure the stresses are uniformly distributed between the loading pins. AWJ, milled and polished samples were tested at 1.5, 15 and 150 mm/min in order to investigate the effect of machining induced damage on flexural properties and fracture mechanisms at different crosshead rates. Flexural strength was calculated as an average of five repeats for each case.

A 2D High Speed DIC (LaVision, GmbH) system was used to measure deformation distribution during flexural tests. The machined edge of the samples were covered by a fine coat of white paint and speckle pattern were created using a Badger 200-3 (USA) airbrush. Davis 10 software (LaVision, GmbH) was used to analyze the surface displacements during testing. The DIC parameters used in the analysis are shown in Table 3. The subset and step pixel sizes were chosen based on an assessment of the mean average speckle and its distribution in order to minimize the systematic error in the analyses. A schematic of the flexural test setup and HS DIC camera view is shown in Figure 1.

Table 3. DIC parameters

Parameter	Value
Technique	2D High Speed DIC
Software	Davis 10
Subset size	27 x 27 pixels
Step size	8 pixels
Camera	Phantom V410L
Lens	100mm Macro lens with 35mm extension tube
Image Resolution	1280 x 800 pixels
Field of view	23.31 x 14.57 mm
Frame Rate	1 to 10 kHz (chosen relative to crosshead displacement rate during flexural testing)
Imaging Distance	166.711 mm
Spatial resolution	0.14 mm

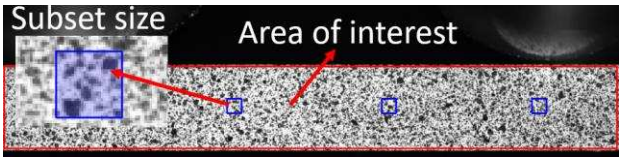

Figure 1. Optical Image of the speckled sample under the 4-point bend test setup showing the area of interest (red rectangle) between the loading points and the selected subset sizes in relation to the produced random speckle pattern indicating the quality of the patterns and suitability of the selected DIC parameters

3. Results and discussion

3.1. Laminate content analysis

Table 4 shows the fibre, resin and void content for manufactured panels where the void content of less than 1% ensures the quality and consistency of the produced panels.

Table 4 - Fibre and resin content (%)

	Resin (%)	Fibre (%)	Voids (%)
Panel 1	36.32	63.15	0.53
Panel 2	38.09	61.25	0.66

3.2. Surface roughness measurements

The average profile roughness (R_a) and the areal average height of the selected area (S_a) of the surface machined by conventional milling and AWJ process are shown in Figure 2. The areal parameters show more information about surface texture compared to profile parameters being more useful in composite surface roughness analysis [29]. R_a and S_a parameters have higher values for samples produced using AWJ. The results of unpaired T statistical tests show that the difference between surface measurements is statistically significant (p-value < 0.05). In addition, a statistical difference is identified for other areal parameters such as S_q, S_p, S_v, S_z and S_{sk} used in surface roughness characterisation between the two manufacturing operations. Samples machined by AWJ had a S_{sk} negative value (-0.561), which represents a surface with deep craters and a few peaks, while milling samples had a positive value (0.023), which shows that surface topography is symmetric. Figure 3 shows 3D surface texture maps of the machined samples. Large craters are observed on the surface machined by AWJ. The initial damage zone happening in AWJ machining creates craters at the entrance of the jet where deep groves are formed and the height profile is at its lowest values (Figure 3 – c).

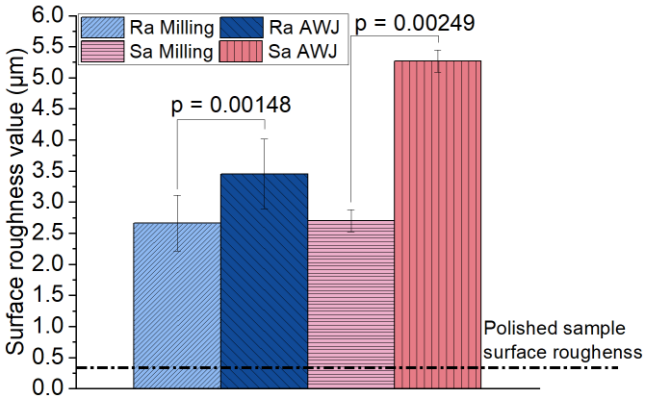

Figure 2. Surface roughness results for samples machined by AWJ and conventional milling displaying standard deviation bars and p-value of T statistical tests

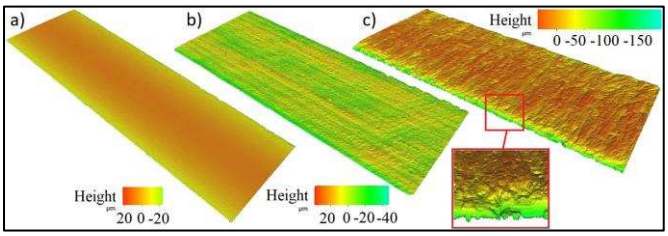

Figure 3. 3D Surface texture maps with height profile (in μm) of surface produced after a) Milling and polishing b) Conventional Milling and c) AWJ machining

3.3. Surface morphology results

The surface machined by AWJ (Figure 4) shows severe damages including fibre pull-out, micro and micro craters, fibre rupture and damage at the entry and exit of the jet. These damages are found across the whole thickness and length of machined samples. The cutting process of AWJ is based on the erosion mechanism taking place at a micro and macro level [9] which can generate these types of damage. Fibre pull-out occurred for the 90° fibre orientation leaving cavities in the surface. Micro craters formed in the 90° fibre orientation due to brittle fracture of fibres at the impact between abrasive particles and fibres, while macro craters form in the 0° orientation due to effect of jet pressure. Both micro and macro craters are affecting the surface roughness measurements. Initial damage zone which occurs at the jet entrance (Figure 4 – e) shows pits and cracks transverse to the jet direction. Due to the position and orientation of these micro cracks, these can represent a delamination initiation point. Furthermore, uncut fibres and micro craters are found at jet exit. No abrasive embedment between the matrix and fibres is noticed.

Surface morphology of milled specimens are in line with previous studies from literature [9, 24, 30, 31]. However, significant matrix smearing was noticed for 90° fibre orientation which might hide the extent of subsurface damage. The 0° fibre orientation areas shows signs of debonding where fibres were lifted up from the surface. Overall, the surface morphology of milled samples showed less damage compared to samples machined by AWJ.

3.4. The effects of machining operations on flexural strength

Figure 5 shows the failure force and flexural strength obtained from mechanical testing. Samples with polished surface experienced the highest force and flexural strength regardless the speed of the test. The trend is followed by samples machined by conventional milling and AWJ. Unpaired T statistical tests results show that differences at a test speed of 1.5 and 15 mm/min are all statistically significant (p-value < 0.05) except for the case between polished and milled specimens (p-value > 0.05).

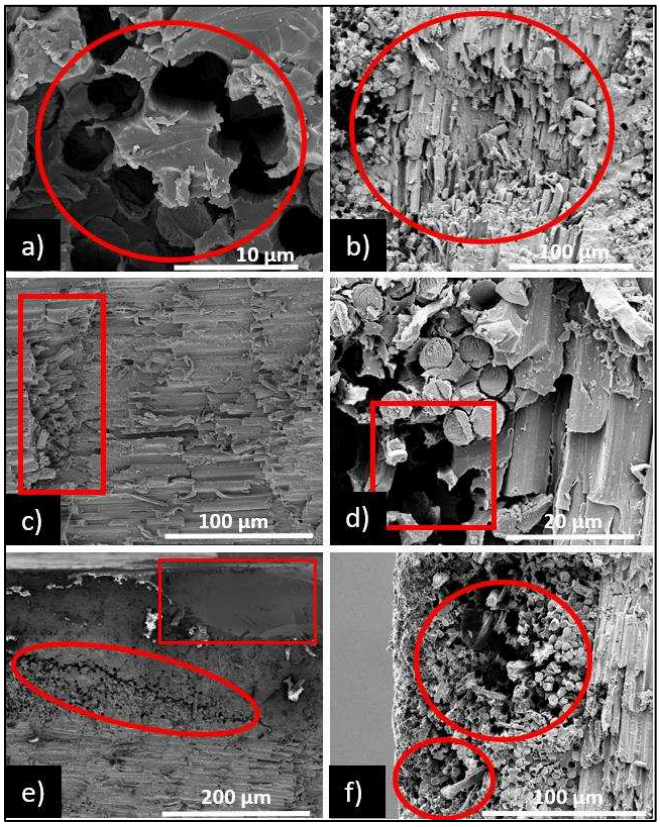

Figure 4. SEM micrographs showing machining induced damage of samples machined by AWJ including a) Individual fibre pull-out b) Removed large bulk of fibre and matrix creating a 'macro crater' c) Uneven jagged fibre fracture d) Fibre cluster pull-out e) Rectangle: Initial damage zone at jet entrance and Ellipse: a transvers crack to jet direction f) Jet exit damage – uncut fibres (small circle) and 'micro crater' formed due to material removal (big circle)

At a speed of 150 mm/min, no statistical difference was found due to variance in test results. The analysis of flexural results using T statistical tests leads to the conclusion that mechanical properties of polished and milled samples are in the same range. This can be attributed to the low extent of surface damage in milled samples. In addition, polished and milled surfaces are free of damage at the edge of specimens (Figure 3 – a, b). On the other hand, AWJ samples experienced the lowest failure force and flexural strength. This can be explained by a possible larger machining induced damage according to the surface texture analysis and observed surface morphology from SEM.

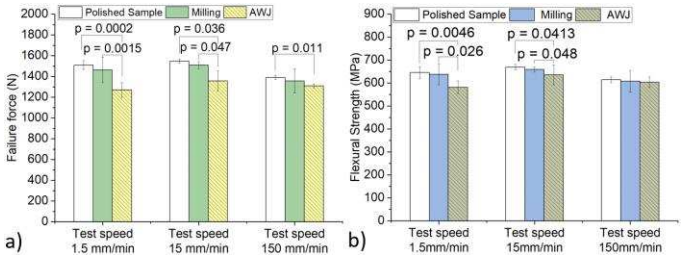

Figure 5. Flexural test results for specimens tested at 1.5, 15 and 150 mm/min displaying standard deviation error bars and p-value of T statistical tests a) Failure force b) Flexural Strength

3.5. Fracture mechanics

The majority of specimens failed by a combination of kinking, matrix cracking and fibre breakage in the compressive side during bending, regardless of the way they have been produced. These failure modes were generated by micro fractures which occurred in different locations across the thickness of specimens depending on the machining process used in manufacturing the test samples. Figure 6 shows initial crack initiation sites within the uniform stress state window of the samples. It was observed that failure initiation sites were populated underneath the loading points for polished samples. These, however, were spread around the top layer for AWJ samples where the major stress is compressive, while milled samples have the initial crack located centrally in the compression side. It was noticed that even the initial crack location is different in each case, the failure and fracture mechanism is similar for all samples.

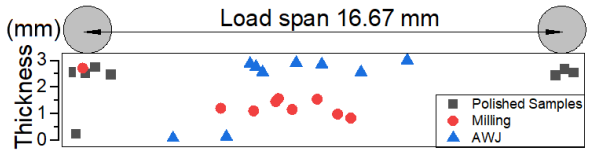

Figure 6. Crack initiation locations

Figure 7 shows the fracture evolution in an AWJ processed sample during the final stages of the loading where the initial crack starts on the top edge (red rectangle in Figure 7 – a). Fibre kinking occurs at the applied compressive stresses (Figure 7 – b). This is attributed to the jet entrance and the initial damage zone which showed micro cracks and pits on the surface close to the edge (Figure 4 – e). The loading is normal to the direction of the generated damage which affected both fibre and matrix. Due to this damage, buckling occurs at lower applied stresses leading to fibre kinking. AWJ processed samples did not fail in the bottom edge tension region as the extension of damage in matrix and fibre is higher at jet entrance. Studies have proved that fibre kinking occurs mainly in areas where are local defects and fibre misalignments[32]. In addition, fibre micro buckling is common for the fibres with small diameter (< 15 um) such as carbon fibres [33]. Shear failure occurs at the interface between fibres and matrix leading to the debonding between fibre and matrix (Figure 7 – b). Crack propagates transverse to ply orientation as a result of fibre buckling, fibre fracture and matrix failure (Figure 7 – c). Catastrophic failure of the samples occurs when the generated crack is long enough and the rest of the material cannot sustain the applied stress as shown in Figure 7 – d. Micro damages located at jet entrance of AWJ samples generated an early start of crack propagation, which produced the bending failure of specimens at lower loading forces. The damage free surface of polished and milled specimens did not generate an early start of crack propagation and lead to better flexural results.

3.6. Deformation evolution analysis

Figure 8 shows maximum normal strain distributions in the tested samples at the onset failure initiation. The high intensity strain contours reveals the possible location of where the specimen starts to crack. AWJ sample (Figure 8 – a) shows a high intensity strain area on the top edge of the specimen which is correlated with the damage zone discussed in the previous section, and once the crack is initiated, the deformation is localized around it (Figure 8 – b) leading to catastrophic failure of the material. On the contrary, the polished samples show the highest measured strains evenly distributed at the top and bottom of the sample, tension and compression sides, respectively (Figure 8 – c).

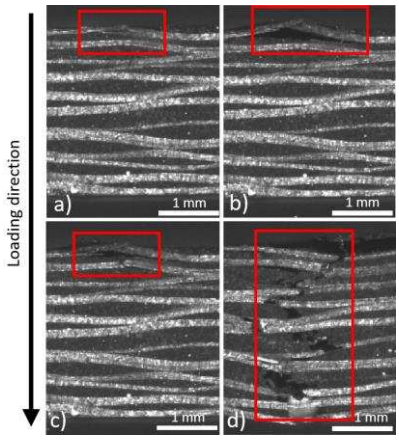

Figure 7. Crack propagation analysis of a sample machined using AWJ a) Initial crack initiation at the top edge of the specimen b) Fibre kinking and debonding c) Transverse crack development c) Final failure

However, the failure could start at the contact point with the loading pins due to fibre/ matrix crushing effect (Figure 8 – d). For milled specimens, strain distribution is uniform with almost no deformation measured at the neutral axis of the samples, as expected, with random fluctuations of the measured strain values (Figure 8 – e). The building of strain contours at crack initiation was progressive, proportional to the crosshead displacement of the loading pins. Maximum strain intensity at crack initiation had a value between 0.8 and 1.2 % for the samples tested. However, after the initial damage, strain contours changed depending on the failure mode, location and size of the initiated crack. In the case of milled specimens (Figure 8 – f) the maximum normal strain contour had a value of 12%, while polished specimens (Fig 10 – d) showed a maximum normal strain of 3.5% around the crack which developed due the compression force applied by the loading nose.

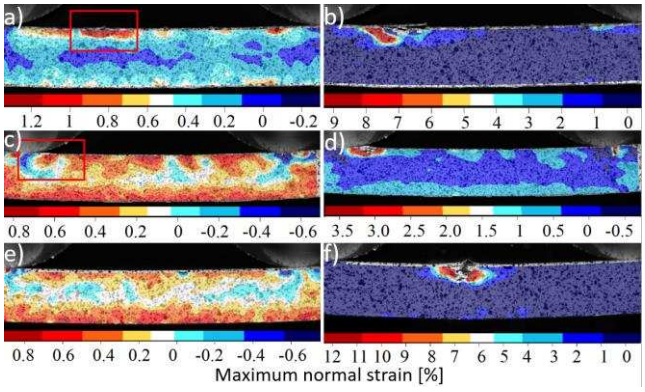

Figure 8. Maximum normal strain distributions in specimens under bending a) AWJ sample before initial crack b) AWJ sample after initial crack c) Polished sample before initial crack d) Polished sample after initial crack e) Milled sample before initial crack f) Milled sample after initial crack

4. Conclusions

- Surface roughness is higher for specimens milled by AWJ process compared to conventional milling. The difference was found statistically significant ($p < 0.05$).
- Surface morphology analysis showed severe damages for samples machined by AWJ. Fibre pull-outs, micro and macro craters were identified across the full thickness of the scanned specimens. Initial damage zone at jet entrance showed pits and transverse micro cracks to jet direction.
- Polished and milled specimens experienced the highest flexural properties followed by AWJ samples. Statistical tests showed a significant difference in flexural results between polished vs AWJ and milled vs AWJ specimens ($p < 0.05$). The low performance of AWJ can be explained by severe machining induced damage illustrated by the surface roughness and morphology.
- Majority of specimens failed by a combination of kinking, matrix cracking and fibre breakage in the compressive side during bending. Crack initiation of samples machined by AWJ is associated with the severe surface damages occurred at jet entrance located on top edge of the samples.
- Strain deformation maps can be used to predict the initial crack location of specimens during 4-point bending tests.

Acknowledgements

The authors would like to acknowledge the EPSRC Industrial Doctorate Centre in Machining Science (EP/L016257/1) for the funding of this work and to Antala, UK for the supply of epoxy resin.

References

1. Hosokawa, A., N. Hirose, T. Ueda,T. Furumoto, High-Quality Machining of Cfrp with High Helix End Mill. *CIRP Annals*, 2014. 63(1): p. 89.
2. Voss, R., L. Seeholzer, F. Kuster,K. Wegener, Influence of Fibre Orientation, Tool Geometry and Process Parameters on Surface Quality in Milling of Cfrp. *CIRP Journal of Manufacturing Science and Technology*, 2017. 18(Supplement C): p. 75.
3. Wang, C., G. Liu, Q. An,M. Chen, Occurrence and Formation Mechanism of Surface Cavity Defects During orthogonal Milling of Cfrp Laminates. *Composites Part B: Engineering*, 2017. 109(Supplement C): p. 10.
4. Arola, D.,M. Ramulu, *A Study of Kerf Characteristics in Abrasive Waterjet Machining of Graphite/Epoxy Composite*. 1996 256.
5. El-Hofy, M., M.O. Helmy, G. Escobar-Palafox, K. Kerrigan, R. Scaife,H. El-Hofy, Abrasive Water Jet Machining of Multidirectional Cfrp Laminates. *Procedia CIRP*, 2018. 68: p. 535.
6. Karunamoorthy, L.,N. Arunkumar, Investigation on Performance of Abrasive Water Jet in Machining Hybrid Composites Au - Selvam, R. *Materials and Manufacturing Processes*, 2017. 32(6): p. 700.
7. Kumaran, S.T., T.J. Ko, M. Uthayakumar,M.M. Islam, Prediction of Surface Roughness in Abrasive Water Jet Machining of Cfrp Composites Using Regression Analysis. *Journal of Alloys and Compounds*, 2017. 724(Supplement C): p. 1037.
8. Ramulu, M.,D. Arola, The Influence of Abrasive Waterjet Cutting Conditions on the Surface Quality of Graphite/Epoxy Laminates. *International Journal of Machine Tools and Manufacture*, 1994. 34(3): p. 295.
9. Sheikh-Ahmad, J.Y., *Machining of Polymer Composites*: Springer Verlag. 2008.
10. El-Hofy, M.H., S.L. Soo, D.K. Aspinwall, W.M. Sim, D. Pearson,P. Harden, Factors Affecting Workpiece Surface Integrity in Slotting of Cfrp. *Procedia Engineering*, 2011. 19: p. 94.
11. Çolak, O.,T. Sunar, Cutting Forces and 3d Surface Analysis of Cfrp Milling with Pcd Cutting Tools. *Procedia CIRP*, 2016. 45: p. 75.
12. Ghidossi, P., M. El Mansori,F. Pierron, Edge Machining Effects on the Failure of Polymer Matrix Composite Coupons. *Composites Part A: Applied Science and Manufacturing*, 2004. 35(7): p. 989.
13. Haddad, M., R. Zitoune, H. Bougherara, F. Eyma,B. Castanié, Study of Trimming Damages of Cfrp Structures in Function of the Machining Processes and Their Impact on the Mechanical Behavior. *Composites Part B: Engineering*, 2014. 57(Supplement C): p. 136.
14. Herring, M.L., J.I. Mardel,B.L. Fox, The Effect of Material Selection and Manufacturing Process on the Surface Finish of Carbon Fibre Composites. *Journal of Materials Processing Technology*, 2010. 210(6): p. 926.
15. Arola, D.,M. Ramula, Machining-Induced Surface Texture Effects on the Flexural Properties of a Graphite/Epoxy Laminate. *Composites*, 1994. 25(8): p. 822.
16. Ramulu, M.,D. Arola, Water Jet and Abrasive Water Jet Cutting of Unidirectional Graphite/Epoxy Composite. *Composites*, 1993. 24(4): p. 299.
17. Doreswamy, D., B. Shivamurthy, D. Anjaiah,N. Sharma, *An Investigation of Abrasive Water Jet Machining on Graphite/Glass/Epoxy Composite*. 2015 1.
18. Hejjaji, A., R. Zitoune, L. Crouzeix, S.L. Roux,F. Collombet, Surface and Machining Induced Damage Characterization of Abrasive Water Jet Milled Carbon/Epoxy Composite Specimens and Their Impact on Tensile Behavior. *Wear*, 2017. 376-377(Part B): p. 1356.
19. Ramalingam, T., S. Bhaskar, K. Seshumadhav,K.V. Allamraju, Optimization of Process Parameters in Bi-Directional Carbon Fiber Composite Using Awjm. *Materials Today: Proceedings*, 2018. 5(9, Part 3): p. 18933.
20. Aparna, M.L., G. Chaitanya, K. Srinivas,J.A. Rao, Fatigue Testing of Continuous Gfrp Composites Using Digital Image Correlation (Dic) Technique a Review. *Materials Today: Proceedings*, 2015. 2(4): p. 3125.
21. Koohbor, B., S. Mallon, A. Kidane,M.A. Sutton, A Dic-Based Study of in-Plane Mechanical Response and Fracture of

Orthotropic Carbon Fiber Reinforced Composite. *Composites Part B: Engineering*, 2014. 66: p. 388.
22. Pollock, P., L. Yu, M.A. Sutton, S. Guo, P. Majumdar,M. Gresil, Full‐Field Measurements for Determining Orthotropic Elastic Parameters of Woven Glass‐Epoxy Composites Using Off‐Axis Tensile Specimens. *Experimental Techniques*, 2012. 38(4): p. 61.
23. Scalici, T., V. Fiore, G. Orlando,A. Valenza, A Dic-Based Study of Flexural Behaviour of Roving/Mat/Roving Pultruded Composites. *Composite Structures*, 2015. 131: p. 82.
24. Ashworth, S., J.P.A. Fairclough, Y. Takikawa, R. Scaife, H. Ghadbeigi, K. Kerrigan,J. Meredith, Effects of Machine Stiffness and Cutting Tool Design on the Surface Quality and Flexural Strength of Edge Trimmed Carbon Fibre Reinforced Polymers. *Composites Part A: Applied Science and Manufacturing*, 2019. 119: p. 88.
25. Ashworth, S., J. Rongong, P. Wilson,J. Meredith, Mechanical and Damping Properties of Resin Transfer Moulded Jute-Carbon Hybrid Composites. *Composites Part B: Engineering*, 2016. 105: p. 60.
26. *Bsi. Geometric Product Specification (Gps) – Surface Texture – Profile Method: Rulesand Procedures for the Assessment of Surface Texture*. BS EN ISO 4288:1998.
27. *Bsi. Geometric Product Specifications (Gps) – Surface Texture: Profile Method –Nominal Characteristics of Contact (Stylus) Instruments.* BS EN ISO 3274:1998.
28. *Astm. Standard Test Method for Flexural Properties of Unreinforced and Reinforcedplastics and Electrical Insulating Materials by Four-Point Bending.*
29. Duboust, N., H. Ghadbeigi, C. Pinna, S. Ayvar-Soberanis, A. Collis, R. Scaife,K. Kerrigan, An Optical Method for Measuring Surface Roughness of Machined Carbon Fibre Reinforced Plastic Composites. 2016.
30. Koplev, A., A. Lystrup,T. Vorm, The Cutting Process, Chips, and Cutting Forces in Machining Cfrp. *Composites*, 1983. 14: p. 371.
31. Duboust, N., H. Ghadbeigi, C. Pinna, S. Ayvar-Soberanis, A. Collis, R. Scaife,K. Kerrigan, An Optical Method for Measuring Surface Roughness of Machined Carbon Fibre- Reinforced Plastic Composites. *Journal of Composite Materials*, 2017. 51(3): p. 289.
32. Rahul, V., S. Alokita, K. Jayakrishna, V.R. Kar, M. Rajesh, S. Thirumalini,M. Manikandan, *3 - Structural Health Monitoring of Aerospace Composites*, in *Structural Health Monitoring of Biocomposites, Fibre-Reinforced Composites and Hybrid Composites*, M. Jawaid, M. Thariq, and N. Saba, Editors. 2019, Woodhead Publishing. p. 33.
33. Giurgiutiu, V., *Chapter 5 - Damage and Failure of Aerospace Composites*, in *Structural Health Monitoring of Aerospace Composites*, V. Giurgiutiu, Editor. 2016, Academic Press: Oxford. p. 125.